Eur. Phys. J. D **11**, 37–44 (2000)

THE EUROPEAN PHYSICAL JOURNAL D

EDP Sciences

Isotope shifts and hyperfine structure in the $[Xe]4f^7 5d\,6s^2\ {}^9D_J \rightarrow [Xe]4f^7 5d\,6s\,6p\ {}^9F_{J+1}$ transitions of gadolinium

K. Blaum[1,a], B.A. Bushaw[2], S. Diel[1], Ch. Geppert[1], A. Kuschnick[1], P. Müller[1], W. Nörtershäuser[2], A. Schmitt[1], and K. Wendt[1]

[1] Institut für Physik, Johannes Gutenberg-Universität Mainz, 55099 Mainz, Germany
[2] Pacific Northwest National Laboratory, Richland, WA 99352, USA

Received 18 November 1999

Abstract. High-resolution resonance ionization mass spectrometry has been used to measure isotope shifts and hyperfine structure in all $[Xe]4f^7 5d\,6s^2\ {}^9D_J \rightarrow [Xe]4f^7 5d\,6s\,6p\ {}^9F_{J+1}$ (J = 2–6) and the $[Xe]4f^7 5d\,6s^2\ {}^9D_6 \rightarrow [Xe]4f^7 5d\,6s\,6p\ {}^9D_5$ transitions of gadolinium (Gd I). Gadolinium atoms in an atomic beam were excited with a tunable single-frequency laser in the wavelength range of 422–429 nm. Resonant excitation was followed by photoionization with the 363.8 nm line of an argon ion laser and resulting ions were mass separated and detected with a quadrupole mass spectrometer. Isotope shifts for all stable gadolinium isotopes in these transitions have been measured for the first time. Additionally, the hyperfine structure constants of the upper states have been derived for the isotopes ^{155,157}Gd and are compared with previous work. Using prior experimental values for the mean nuclear charge radii, derived from the combination of muonic atoms and electron scattering data, field shift and specific mass shift coefficients for the investigated transitions have been determined and nuclear charge parameters λ for the minor isotopes ^{152,154}Gd have been calculated.

PACS. 32.10.Fn Fine and hyperfine structure

1 Introduction

The ultimative objective of our work is the development of a method for sensitive ultratrace determination of stable isotopes of gadolinium using resonance ionization mass spectrometry (RIMS), which will have applications in a number of fields.

(1) In cosmochemical studies, the ratio of the minor stable isotopes ^{152}Gd/^{154}Gd in presolar grains from meteorites is of interest since it can be used to determine the temperature of the stellar environment during the formation of these isotopes [1–3]. However, conventional thermal-ionization mass spectrometry is limited by isobaric interference from ^{152}Sm and only a few limited results are available [4].
(2) Because of the large thermal neutron capture cross sections of the odd isotopes ^{157,155}Gd (σ = 254 and 60.9 kbarns, respectively [5]), these isotopes can serve as sensitive indicators of integrated thermal neutron exposures in a variety of samples and neutron-capture effects in meteorites [6,7].
(3) In medicine gadolinium diethylenetriamine pentaacetic acid (Gd-DTPA) chelate is used as the primary contrast medium for magnetic resonance imaging (MRI) [8,9], but little is known about the kinetics and physiological effects of Gd in the human body ([9] and references therein), thus there is a need to determine the concentration of Gd in blood and human tissue.

In addition to these analytical applications, an efficient excitation scheme for multi-step resonance ionization might be used for enrichment of the odd gadolinium isotopes ^{155,157}Gd, which are used as burnable poison in nuclear reactors [10,11]. Due to this wide range of interest, we chose Gd as a test candidate for adapting our diode-laser-based resonance ionization mass spectrometer [12,13] to the detection of rare earth elements. For the different applications, optical one-, two- or three-step resonance excitation and subsequent ionization will be applied with the goal of attaining elemental and isotopic selectivities of $> 10^6$ and high overall detection efficiencies of up to 10^{-4}. Hence, we have investigated six resonance lines of Gd I in the wavelength range of 422–429 nm that might serve as a first resonant step in such ionization schemes. This wavelength range is accessible for diode-laser-based RIMS since it can be reached either by efficient frequency doubling of a powerful infrared diode laser at about 850 nm [14] or by directly using one of the blue diode lasers which have recently become available [15].

[a] e-mail: K.Blaum@Larissa.physik.uni-mainz.de

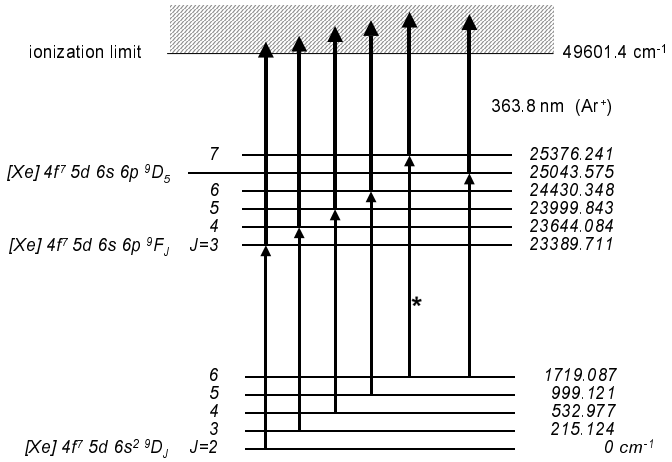

Fig. 1. Investigated transitions and related energy levels of Gd I. The transition which has been measured using a frequency-doubled diode laser is marked with an asterix.

Hyperfine structure (HFS) constants of the various ground state fine structure components have been measured previously at high precision by atomic beam laser spectroscopy [16] while upper states HFS constants, which have been determined by Doppler-free laser fluorescence spectroscopy [17], are less precise with a relative uncertainty of about 1%. Furthermore, there are no prior measurements of isotope shifts (IS) in the investigated transitions. However, isotope shifts in other transitions are reported in [16,18] where they were used to evaluate the J dependence of isotope shifts and hyperfine structure and to extract changes in the nuclear charge distribution. Some of these and other measurements have recently been combined with K X-ray, electron scattering, and muonic atom data to obtain more reliable information about the nuclear charge distribution ([19] and references therein). In this paper we report high-resolution laser spectroscopic measurements of the IS for all stable isotopes of Gd in all five possible $[\mathrm{Xe}]4f^7 5d\,6s^2\ {}^9\mathrm{D}_J \rightarrow [\mathrm{Xe}]4f^7 5d\,6s\,6p\ {}^9\mathrm{F}_{J+1}$ (J = 2–6) transitions as well as in the $[\mathrm{Xe}]4f^7 5d\,6s^2\ {}^9\mathrm{D}_6 \rightarrow [\mathrm{Xe}]4f^7 5d\,6s\,6p\ {}^9\mathrm{D}_5$ transition. These measurements were performed using RIMS in a well-collimated atomic beam. The excitation and ionization scheme is shown in Figure 1. The resonant excitation is followed by non-resonant ionization with a 363.8 nm line of an argon ion laser. The HFS pattern of the odd isotopes ^{155,157}Gd is complex and incompletely resolved, therefore, a sophisticated fitting routine [20] was used to obtain the IS of the center of gravity (cg) of the HFS as well as the upper state HFS coupling constants. The uncertainties of the HFS constants were reduced in comparison to [17] and are in good agreement with results given in [21]. Using the measured IS, field shift and specific mass shift constants are derived by using a King plot procedure with experimental-data-based, model-independent values of the mean nuclear charge parameter λ which are available for the major gadolinium isotopes ^{160,158,157,156,155}Gd. We found unexpectedly large specific mass shift constants, which may be responsible for the systematic discrepancy between λ values found by combined analysis of electron scattering and muonic atom transition energies [19] and purely optical measurements [18]. Additionally, we used the King plots to determine values for the change in nuclear charge radii of ^{154,152}Gd, for which no reliable experimental electron scattering and muonic atom data are available.

2 Experimental

A schematic of the resonance ionization mass spectrometer is shown in Figure 2. It can be divided into three major components: a graphite crucible for sample atomization, the laser system for multi-step resonant excitation and ionization of the neutral atoms, and a quadrupole mass spectrometer (QMS) system for mass separation and ion detection.

In experiments described here, samples of metallic gadolinium have been placed in an electrothermally heated graphite crucible, which functions as a self-collimating canal atomic beam source. Typical operating temperatures of the crucible were 1300–1800 °C. The crucible exit orifice was located $\sim$ 20 cm away from the ionization region, where a 3 mm entrance aperture limited the atomic beam divergence to $\sim$ 1° (full angle). The laser beam used for resonant excitation intersects the atomic beam at right angle within the QMS ionizer. Ions created in the ionization region are extracted with conventional ion optics and analyzed with a commercial QMS (ABB Extrel, Pittsburgh, USA). Ions passing through the mass filter are detected with an off-axis channeltron particle multiplier operated in ion counting mode. The residual gas pressure in the vacuum chamber was about 5×10^{-7} mbar, even during the heating of the crucible. A detailed description of the crucible-QMS system has already been given in [22,23].

Two different laser systems were used for the resonant excitations. The $6s^2\ {}^9\mathrm{D}_6 \rightarrow 6s\,6p\ {}^9\mathrm{F}_7$ resonance transition (422.7 nm, marked with * in Fig. 1) was studied using a tunable diode laser, frequency-doubled with a $KNbO_3$ crystal in an actively stabilized external ring cavity. The other transitions were investigated using a ring dye laser (Coherent 699-21) operated with stilbene-3 and pumped with the UV lines of an argon ion laser. Non-resonant photoionization of the excited atoms was accomplished in both cases with 0.5–0.9 W of 363.8 nm laser radiation from a separate argon ion laser. The short-term frequency jitter of both tunable laser systems used for resonant excitation is less than 500 kHz. Medium- to long-term (> 0.1 s) frequency drift stabilization, as well as frequency tuning was provided by computer-controlled fringe-offset-locking [24,25] using a temperature-stabilized confocal Fabry-Perot interferometer (CFI), referenced to a stabilized single-frequency He:Ne laser. Long-term frequency drift is limited by the stability of the He:Ne laser and has been measured as $<$ 3 MHz/day. Accurate knowledge of the CFI free spectral range is required for high precision frequency scans. This was obtained by measuring the ^{133}Cs ground state HFS in a single-resonance experiment analogous to those reported here for Gd.

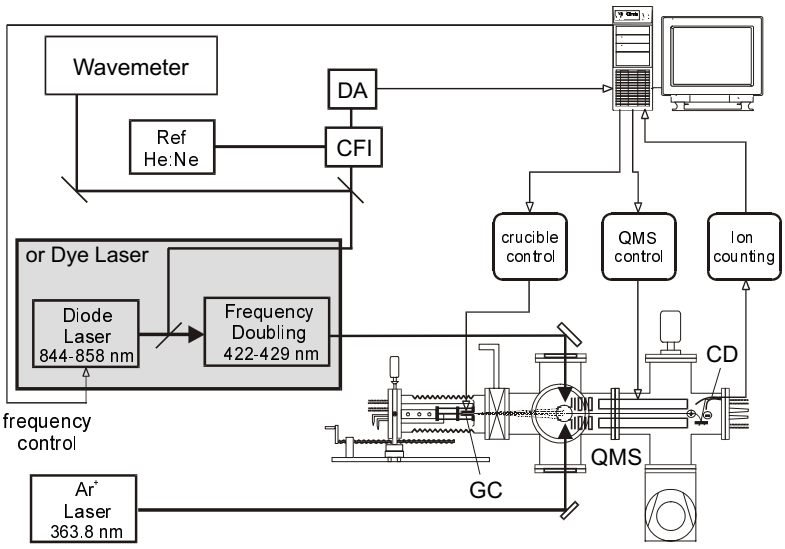

Fig. 2. Schematic diagram of the experimental setup showing the vacuum chamber with the graphite crucible (GC), quadrupole mass spectrometer system (QMS), and off-axis channeltron detector (CD) as well as the laser system together with the confocal Fabry-Perot interferometer (CFI) and the detector assembly (DA). For the resonance transitions either a frequency doubled diode laser or an argon ion pumped dye laser was used.

3 Results and discussion

3.1 Isotope shift of even isotopes

Isotope shifts of the even isotopes were determined with no DC bias on the mass spectrometer poles which allows transmission of all masses. The frequency of the resonant laser was scanned in 10 MHz steps and a typical experimental spectrum is shown on a semilogarithmic scale in Figure 3. The HFS of the two odd isotopes ^{155,157}Gd is not resolved and will be considered separately below, however, the main HFS components are clearly separated from the peaks of the neighboring even massed isotopes in all transitions except $6s^2\ ^9\mathrm{D}_6 \rightarrow 6s\,6p\ ^9\mathrm{D}_5$. Thus, except for this transition, all even mass isotope shifts were measured in the same scan without mass resolution. In some weaker transitions, the resonance signals from the two least abundant isotopes (^{152,154}Gd, abundance $2.1606(9)\times10^{-2}$ and $2.029(5)\times10^{-3}$, respectively [26]) were recorded at higher oven temperatures, and consequently higher atomic beam flux, for improved signal-to-noise ratio. Systematic errors caused by non-perpendicular geometry between laser beam and atomic beam, and corresponding mass dependent Doppler shifts, were avoided by using a procedure that retroreflects the resonance laser beam [27] and reduces the angular deviation to $\leq 0.2°$, which corresponds to a systematic error < 10 kHz/amu.

Peak positions were determined by fitting Voigt profiles to the experimental data using statistical weighting. Individual linewidths parameters were free variables to allow for the unresolved ^{155,157}Gd HFS. A typical fit is shown as the solid line in Figure 3, it is obvious that the experimental data is well-described by the Voigt profiles. The Lorentzian contribution to the total widths depends on the transition and varied between 18 and 27 MHz (FWHM), corresponding to lifetimes of 6 to 9 ns for the different $6s\,6p\ ^9\mathrm{F}_J$ states. The Gaussian contribution is determined by the oven temperature and the divergence of the atomic beam and was typically 10 MHz (FWHM).

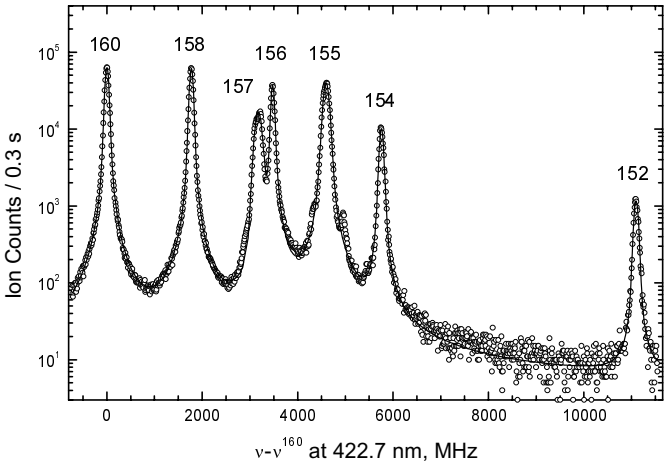

Fig. 3. Spectrum of the $6s^2\ ^9\mathrm{D}_6 \rightarrow 6s\,6p\ ^9\mathrm{F}_7$ transition for all stable gadolinium isotopes. Experimental result is shown as data points with Voigt-profile fits as solid lines. Laser detunings are given relative to the ^{160}Gd resonance. The QMS was operated in the RF-only mode to allow the transmission of all masses.

The IS are calculated with respect to ^{160}Gd as the reference isotope and uncertainties are given as standard error of the mean of five measurements (9–15 measurements for the transition observed with the diode laser). Combined results for all measurements are given in Table 1 including the IS of the odd isotopes, which were obtained from HFS fits discussed below. It should be noted that the IS between ^{154}Gd and ^{152}Gd is about 3 times larger than the shift between ^{160}Gd and ^{158}Gd. This anomalously large shift is attributed to the spontaneous symmetry breaking between the neutron number 88 and 90 and the resulting transition from a spherical to a deformed nucleus, as has been previously observed and described in ^{152}Sm–^{150}Sm [28]. Furthermore, the cg of the HFS of ^{157}Gd lies closer to ^{156}Gd than to ^{158}Gd, while the ^{155}Gd cg lies nearly

Table 1. Measured isotope shifts ($\nu^A - \nu^{160}$) in the investigated [Xe]$4f^7 5d\,6s^2 \rightarrow$ [Xe]$4f^7 5d\,6s\,6p$ transitions of gadolinium. All values in MHz. Uncertainties estimated for this work are given as the standard error of the mean. IS of the odd isotopes are given for the center of gravity (cg) obtained from HFS fits.

Transition	^{158}Gd	^{157}Gd (cg)	^{156}Gd	^{155}Gd (cg)	^{154}Gd	^{152}Gd
$^9D_6 \rightarrow {}^9F_7$	1 769.7(12)	3 176.4(21)	3 470.8(14)	4 648.5(15)	5 770.2(16)	11 093.1(18)
$^9D_5 \rightarrow {}^9F_6$	1 776.1(13)	3 222.1(15)	3 487.1(15)	4 686.8(14)	5 833.1(23)	11 387.3(32)
$^9D_4 \rightarrow {}^9F_5$	1 689.5(13)	3 024.7(15)	3 319.6(14)	4 439.6(13)	5 511.5(21)	10 530.7(31)
$^9D_3 \rightarrow {}^9F_4$	1 730.9(15)	3 091.6(17)	3 398.4(17)	4 543.9(18)	5 637.0(23)	10 751.0(33)
$^9D_2 \rightarrow {}^9F_3$	1 758.4(17)	3 140.6(19)	3 452.8(20)	4 616.9(22)	5 727.0(23)	10 906.6(30)
$^9D_6 \rightarrow {}^9D_5$	1 903.8(7)	3 447.3(8)	3 729.6(10)	5 013.3(10)	6 229.5(13)	12 150.2(21)

equidistant between ^{156}Gd and ^{154}Gd, which is also a manifestation of the nuclear conformation changes.

3.2 Isotope shift and hyperfine structure of ^{155,157}Gd

The odd isotopes ^{155}Gd and ^{157}Gd both have a nuclear spin of $I = 3/2$, which gives rise to HFS splitting in all atomic states with non vanishing angular momentum J. The energy shift of each component with respect to the reference isotope can be calculated by [29]

$$\Delta E_{\mathrm{F}} = \Delta\nu_{\mathrm{IS}} + \frac{A}{2}C + \frac{B}{4}\frac{\frac{3}{2}C(C+1) - 2I(I+1)J(J+1)}{(2I-1)(2J-1)IJ} \tag{1}$$

where $\Delta\nu_{\mathrm{IS}}$ is the IS of the center of gravity of the HFS, $C = F(F+1) - I(I+1) - J(J+1)$ is the Casimir factor, A is the magnetic dipole coupling constant, and B is the electric quadrupole coupling constant.

Experimental hyperfine spectra were recorded with the mass spectrometer operating in mass resolved mode to obtain isotopically pure spectra and therefore avoid interference from the even isotope ^{156}Gd. The laser was scanned in 2 MHz steps across all HFS components and reference to an even isotope was made by switching the QMS to record a spectrum of either ^{156}Gd or ^{160}Gd, between successive HFS scans. Figure 4 shows examples of the experimentally observed spectra for ^{157}Gd (a) and ^{155}Gd (b). The ^{156}Gd reference spectra are also included in the figure. In all cases the HFS is not completely resolved and a sophisticated fitting procedure was necessary to extract reliable values for the HFS coupling constants and the IS. A nonlinear-least-squares procedure, based on the MINUIT code [30], starts with a set of initial input fitting parameters, which include the A and B factors of both states, Gaussian and Lorentzian linewidth components, the overall intensity, an energy shift of the center of gravity and a baseline offset. These values are then used to calculate an initial hyperfine spectrum, assuming equal Voigt width parameters for all hyperfine components, and intensity ratios that follow the theoretical prediction given in [31]. The calculated pattern is then iteratively compared to the experimental data with adjustment of the input parameters for χ^2-minimization. In most transitions we found that the A and B factors of the lower and upper states are strongly correlated, and hence there is limited confidence in the resulting coupling constants when all of them are left as free fitting parameters. This problem was solved by fixing the more precisely known A and B factors of the ground states [16], while the less precise results of [17] for the upper states were used as starting parameters for minimization. For consistency, this procedure for removing parameter correlations

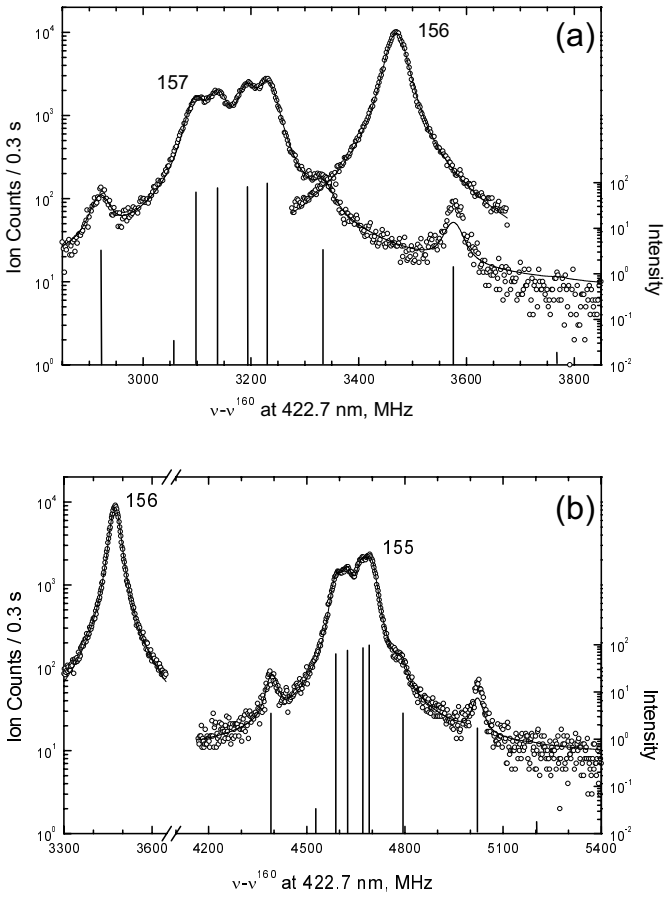

Fig. 4. Spectra showing IS and HFS for the isotopes ^{157}Gd (a) and ^{155}Gd (b) in the $6s^2\ {}^9D_6 \rightarrow 6s\,6p\ {}^9F_7$ transition. Laser detunings are given relative to the ^{160}Gd resonance. The QMS was used to obtain isotopically pure spectra. For ^{156}Gd the solid curves are fits using Voigt profiles, for the odd gadolinium isotopes a fitting routine described in the text was used. Note that the scale for the theoretical intensities on the right is compressed with respect to the scale of the experimental data.

Table 2. Hyperfine structure constants for ^{155}Gd and ^{157}Gd in the excited $6s\,6p\ ^9\mathrm{F}_J$ ($J = 3$–7) and $6s\,6p\ ^9\mathrm{D}_6$ states. All values are in MHz. Uncertainties in the first parentheses are purely statistical from the HFS fitting results, given as standard error of the mean. The uncertainty given in the second parentheses includes error propagation from the fixed ground state coupling constants taken from [16].

State	Author	A(^{155}Gd)	B(^{155}Gd)	A(^{157}Gd)	B(^{157}Gd)
	this work	−6.69(1) (19)	590.7(3) (27)	−8.60(1) (22)	629.9(4) (35)
$6s\,6p\ ^9\mathrm{F}_7$	[17]	−6.7(4)	592(8)	−8.5(4)	632(8)
	[21]	−6.61(15)	596.2(37)	−8.66(19)	635.1(39)
	this work	−41.50(5) (26)	348.3(1) (42)	−54.54(3) (17)	372.1(7) (33)
$6s\,6p\ ^9\mathrm{F}_6$	[17]	−41.5(4)	348(8)	–	–
	[21]	−41.51(25)	351.0(27)	−54.43(34)	373.9(29)
	this work	−10.39(3) (12)	−72.7(5) (13)	−13.77(3) (17)	−79.0(8) (20)
$6s\,6p\ ^9\mathrm{F}_5$	[17]	−10.6(4)	−78(8)	−13.6(4)	−80(8)
	[21]	−10.46(19)	−75.2(22)	−13.72(25)	−80.2(24)
	this work	−7.12(11) (21)	−248(2) (3)	−9.22(10) (19)	−265.5(18) (23)
$6s\,6p\ ^9\mathrm{F}_4$	[17]	−7.6(4)	−248(8)	9.2(4)	−266(8)
	[21]	−7.29(24)	−248.2(34)	−9.55(34)	−264.2(36)
	this work	1.69(5) (23)	−288.2(12) (16)	2.31(3) (16)	−311.1(5) (14)
$6s\,6p\ ^9\mathrm{F}_3$	[17]	2.3(4)	−295(8)	2.3(4)	−295(8)
	[21]	1.84(12)	−293.9(25)	2.40(14)	−313.6(27)
	this work	−29.19(6) (52)	409.6(3) (60)	−37.82(1) (30)	440.5(9) (34)
$6s\,6p\ ^9\mathrm{D}_5$	[17]	−28.9(4)	412(8)	−37.9(4)	439(8)
	[21]	−29.20(23)	410.4(41)	−38.29(30)	437.1(43)

was used for all transitions and the fitting then converged very well, reaching reduced χ^2 values in the range of 1–2 assuming a purely statistical error. In Figure 4, the fitted spectra are shown as solid lines and good agreement with the experimental data is observed. The positions and intensities of each hyperfine component, as derived from the fitting routine, is also included in the figure with the strongest component normalized to 100. While the intensity rules given in [31] are only strictly valid in the case of pure RS coupling, the HFS intensity patterns were generally well-reproduced in all investigated transitions, with only some of the weakest components somewhat stronger than expected.

Each recorded spectra was fitted separately and the resulting A and B constants as well as the IS (Tab. 1) were averaged. Table 2 lists the derived HFS coupling constants for the different upper states. The uncertainties in the first parentheses are the standard deviations of our results for a set of (in most cases) five measurements. The value in the second set of parenthesis includes propagation of the uncertainty reported by [16] for the lower state. This uncertainty had only a negligible influence on the isotope shift results. The observed upper state HFS coupling constants agree well with the results from [17] but uncertainties have been reduced by about a factor of 2 to 3. The results also agree well with unpublished values from Klemz' Ph.D. thesis [21].

3.3 Determination of isotope shift constants

For a given transition, the isotope shift between two isotopes with atomic masses A and A' can be described as the sum of the mass shift (MS) and the nuclear-shape dependent field shift (FS) [19]:

$$\delta\nu^{A,A'} = F\lambda^{A,A'} + M\frac{A - A'}{AA'} \tag{2}$$

where F is the field shift coefficient and $\lambda^{A,A'}$ describes the change of the radial nuclear charge parameters, which is dominated by the change in mean-square nuclear charge radii $\delta\langle r^2\rangle^{A,A'}$. The contribution of the higher radial moments to $\lambda^{A,A'}$ is about 5% in Gd [19]. By convention, the mass shift constant M is separated into the normal mass shift (NMS) constant and the specific mass shift (SMS) constant, $M = M_{\mathrm{NMS}} + M_{\mathrm{SMS}}$. The NMS constant is easily calculated from

$$M_{\mathrm{NMS}} = \nu_0\frac{m_{\mathrm{e}}}{m_{\mathrm{u}}} = \frac{\nu_0}{1\,822.8} \tag{3}$$

where ν_0 is the transition frequency. The SMS, which arises from electron-correlation, has the same functional form as the NMS but its magnitude is difficult to evaluate theoretically. The NMS can be subtracted from the total IS to yield the residual isotope shift (RIS), $\delta\nu_{\mathrm{RIS}}^{AA'}$.

Table 3. Change of the nuclear charge parameter $\lambda^{A,A'}$ either derived from muonic atom and electron scattering data [19] or from optical isotope shift measurements with theoretical estimation of F and M_{SMS} [18]. All values are in fm^2.

Ref.	$\lambda^{160,158}$	$\lambda^{158,157}$	$\lambda^{157,156}$	$\lambda^{156,155}$	$\lambda^{155,154}$	$\lambda^{154,152}$
[19]	0.1636(62)	0.1178(62)	0.0361(62)	0.1013(61)	–	–
[18]	0.1345(72)	0.1044(72)	0.0256(15)	0.0883(102)	0.0843(45)	0.388(20)

Introduction of the RIS into equation (2) and multiplication with the mass factor $AA'/(A'-A)$ leads to the linear relation

$$\delta\nu_{\mathrm{RIS}}^{AA'}\frac{AA'}{A-A'} = M_{\mathrm{SMS}} + F\lambda^{AA'}\frac{AA'}{A-A'}\,. \qquad (4)$$

When $\delta\nu_{\mathrm{RIS}}^{AA'}$ and $\lambda^{A,A'}$ are multiplied by the mass factor, they are referred to as the modified RIS and modified $\lambda^{A,A'}$, respectively. This linear relationship (4) can be used either to determine M_{SMS} and F or to evaluate the nuclear charge parameter $\lambda^{A,A'}$. In the latter case, the IS constants have to be known and are usually estimated by semiempirical methods (*e.g.* Goudsmit-Fermi-Segré) or *ab initio* calculations using self-consistent-field procedures. This approach has been used to estimate $\lambda^{A,A'}$ values for all stable isotopes of Gd [18,32]. While it can yield very precise relative values of λ, the theoretical estimation of F and M_{SMS} leads to relative large uncertainties in the absolute values. If, on the other hand, $\lambda^{A,A'}$ values are established from methods such as measurements of transition energies in muonic atoms or elastic electron scattering, these can be used to determine the IS constants. It has recently been shown that the combination of muonic and electron scattering data yields nearly model-independent $\lambda^{A,A'}$ values which are impressively consistent with results from K X-ray experiments [19]. The set of $\lambda^{A,A'}$ values obtained by this method for the isotopes $^{160-155}$Gd was used in the following analysis and is given in Table 3. Additionally the optically derived $\lambda^{A,A'}$ results from [18], which were mentioned above, are included in the table. These are systematically smaller by about 15%, an observation which is addressed below. We chose the $\lambda^{A,A'}$ values from [19] for our determination of the mass shift and field shift constants, since they are based only on experimental data.

Plotting the modified RIS *versus* the modified $\lambda^{A,A'}$ values according to equation (4) (King plot [33]), yields the expected linear dependence with a y intercept of modified M_{SMS} and slope of F. As an example this plot is shown for the $6s^2\ ^9\mathrm{D}_6 \rightarrow 6s\,6p\ ^9\mathrm{F}_7$ transition in Figure 5, where the scales have been normalized with the inverse mass factor of the reference isotope pair ^{158,160}Gd. This normalization to an arbitrarily chosen standard pair of isotopes facilitates the reading of the King plot diagram. The straight line is the result of a linear regression with error weighting in both coordinates. M_{SMS} and F values, derived from the analysis, are summarized in Table 4. The χ^2 value for the straight line fitting ranged between 0.3 and 0.4, indicating that the uncertainties for the $\lambda^{A,A'}$ values are overestimated. Therefore, the error of the fitting result was adjusted by multiplication with the square root of χ^2. The relative uncertainty of F is about 7%, while that of M_{SMS} is much larger and typically around 35%. The negative field shift factor reflects the fact that the optical frequencies decrease while the rms nuclear radii of the Gd isotopes increases with increasing neutron number. Hence $\lambda^{A,A'}$ is positive if $A > A'$ and the field shift in an $s \rightarrow p$ transition is negative [19].

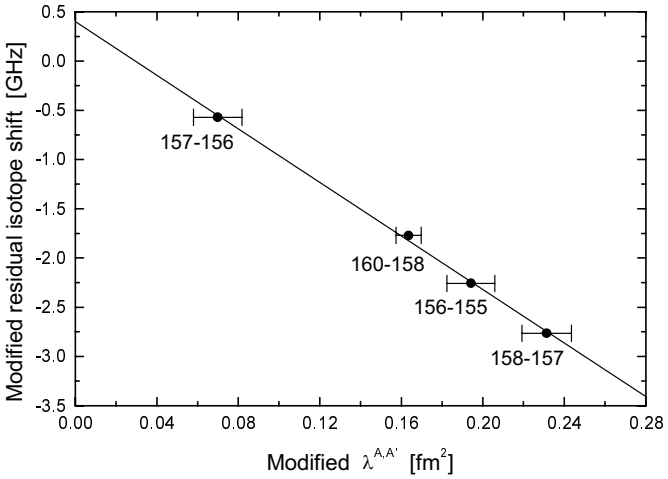

Fig. 5. "Modified residual isotope shifts" in the $6s^2\ ^9\mathrm{D}_6 \rightarrow 6s\,6p\ ^9\mathrm{F}_7$ transition *versus* "modified $\lambda^{A,A'}$ parameter" from [19]. For normalization ^{160}Gd–^{158}Gd is used as reference isotope pair, *i.e.* x- and y-values are multiplied with the inverse mass factor $(A'-A)/A'A$ where $A' = 160$ u and $A = 158$ u. Linear regression analysis (solid line) was used to obtain specific mass shift and field shift coefficients.

It should be noted that the SMS is rather large, in all transitions it is 10 to 20 times larger than the corresponding NMS. This is in contrast to the expectation that $ns \rightarrow np$ and $ns^2 \rightarrow ns\,np$ transitions have small SMS contributions ($M_{\mathrm{SMS}}/M_{\mathrm{NMS}} \leq 0.9$) and only transitions with a change in the number of d or f electrons have $M_{\mathrm{SMS}} \gg M_{\mathrm{NMS}}$ [34]. However, the upper states of the investigated transitions have large admixtures of the $4f^7 5d^2 6p$ configuration [35] which may give rise to the observed large SMS. Furthermore, it should be mentioned that the derivation of the $\lambda^{A,A'}$ values in [19] was hampered by the fact that electron scattering data is only available for the isotope ^{158}Gd. Therefore the radial moment ratios $V_{\mathrm{n}}^{\mathrm{e}}$ which connect the different characteristic radial moments determined by different methods, were assumed to be isotope independent though they are known to vary slightly within an isotopic chain [19]. However, these corrections are rather small and repeated analysis,

Table 4. Isotope shift constants and change of the mean nuclear charge parameters for the isotopes ^{152,154}Gd in the investigated $[\mathrm{Xe}]4f^7 5d\,6s^2 \rightarrow [\mathrm{Xe}]4f^7 5d\,6s\,6p$ transitions of gadolinium. Uncertainties are standard deviations from the linear regression analysis of the modified residual isotope shift *vs.* modified $\lambda^{A,A'}$ data.

Transition	M_{NMS} (GHz amu)	M_{SMS} (THz amu)	$M_{\mathrm{SMS}}/M_{\mathrm{NMS}}$	F (GHz/fm^2)	$\lambda^{155,154}$ (fm^2)	$\lambda^{154,152}$ (fm^2)
$^9\mathrm{D}_6 \rightarrow {}^9\mathrm{F}_7$	389.1	5.0(1.7)	13(4)	−13.64(79)	0.099(2)	0.424(12)
$^9\mathrm{D}_5 \rightarrow {}^9\mathrm{F}_6$	385.3	6.6(2.0)	17(5)	−14.47(93)	0.100(2)	0.425(13)
$^9\mathrm{D}_4 \rightarrow {}^9\mathrm{F}_5$	385.9	4.2(1.7)	11(4)	−12.75(77)	0.099(2)	0.425(13)
$^9\mathrm{D}_3 \rightarrow {}^9\mathrm{F}_4$	385.3	4.1(1.6)	11(4)	−12.93(76)	0.099(2)	0.425(12)
$^9\mathrm{D}_2 \rightarrow {}^9\mathrm{F}_3$	384.7	4.1(1.7)	11(4)	−13.13(78)	0.099(2)	0.424(12)
$^9\mathrm{D}_6 \rightarrow {}^9\mathrm{D}_5$	383.6	7.0(2.0)	18(5)	−15.46(93)	0.099(2)	0.424(12)

assuming a linear change of $V_{\mathrm{n}}^{\mathrm{e}}$ along the isotopic chain, does not yield significantly smaller SMS factors [36].

The $\lambda^{A,A'}$ values calculated by [18] rely on the assumption that the SMS is essentially 0 for their reference transition. However, a large SMS could cause a significant change in their results and might explain the systematic discrepancy between the two rows in Table 3. Therefore, the IS data of the reference transition of [18] were analyzed by the same King plot procedure used in this paper and a comparable large SMS ($M_{\mathrm{SMS}}/M_{\mathrm{NMS}} \approx 7$) was found. It appears that their assumption of $M_{\mathrm{SMS}} \approx (0 \pm 0.5) M_{\mathrm{NMS}}$ (taken from [32] which lists similarly small $\lambda^{A,A'}$ values) was not warranted, while their estimation of the FS constant $F \approx -8.26$ GHz/fm^2 agreed very well with our fitting result of $F = -8.0(8)$ GHz/fm^2. To determine the size of the error introduced by the non-negligible SMS, the calculation of $\lambda^{A,A'}$ from the IS data of [18] has been repeated, taking the SMS into account but still using the theoretically estimated F value. The obtained $\lambda^{A,A'}$ values are closer to the values from [19] and more evenly distributed, *i.e.* some are larger, others are smaller. Hence, the discrepancy in the $\lambda^{A,A'}$ values as derived in [18,32] is removed by assuming a large SMS as observed in this work.

The isotopes ^{154,152}Gd are not included in the King plot, since there is no reliable data for $\lambda^{155,154}$ and $\lambda^{154,152}$ [19,35]. However, we extrapolate these values from our IS measurements taking advantage of the linear relationship between the modified IS and the modified $\lambda^{A,A'}$. This has been done for every transition and the results are given in Table 4. The agreement between the different transitions is excellent. The standard deviation of the six measurements is less than 1%, which reflects the precision of the isotope shift measurements. Additionally, the same procedure was carried out for the Gd IS data presented in [18], representing another 8 transitions in a different manifold of lines. For all 14 transitions the results agree very well with a standard deviation of less than 1%. The uncertainty of the derived $\lambda^{155,154}$ values is calculated using Gaussian error propagation. The average values are $\lambda^{155,154} = 0.099(2)$ fm^2 and $\lambda^{154,152} = 0.425(13)$ fm^2 and the uncertainties are consistent in magnitude with those given in the first row of Table 3. As expected, the results are about 15% larger than the purely optical values given in [18]. They are also in very good agreement with previously reported values of $\lambda^{155,154} = 0.093(3)$ fm^2 and $\lambda^{154,152} = 0.434(50)$ fm^2 [37] which were derived by a model-dependent analysis of combined optical IS measurements and electron and muonic X-ray data.

4 Summary

Resonance ionization mass spectrometry has been used for spectroscopic studies on all stable isotopes of gadolinium, with precise isotope shift and hyperfine structure measurements in all five

$$[\mathrm{Xe}]4f^7 5d\,6s^2\ ^9\mathrm{D}_J \rightarrow [\mathrm{Xe}]4f^7 5d\,6s\,6p\ ^9\mathrm{F}_{J+1} \quad (J = 2\text{–}6)$$

and the

$$[\mathrm{Xe}]4f^7 5d\,6s^2\ ^9\mathrm{D}_6 \rightarrow [\mathrm{Xe}]4f^7 5d\,6s\,6p\ ^9\mathrm{D}_5$$

transitions. All isotope shifts were measured for the first time and with a relative accuracy of better than 10^{-3}. By fitting the hyperfine formula with assumed Voigt profiles to the experimental observed hyperfine patterns of ^{155}Gd and ^{157}Gd, we obtained precise A and B hyperfine coupling constants for the upper states involved in the transitions. Agreement with prior hyperfine structure results is very good and uncertainties have been reduced. Isotope shift results for all isotopes have been used to extract specific mass shift and field shift constants by King plot procedures. Also, precise values for the change in nuclear charge radii of the minor isotopes ^{152}Gd and ^{154}Gd have been obtained. The precise knowledge of the IS and HFS in the investigated transitions is an essential precursor for the development of multiple resonance ionization schemes that will yield the required sensitivity for ultra-trace analysis of gadolinium.

The authors would like to thank Professor G. Fricke and Professor E.-W. Otten for stimulating discussions. Funding from the Deutsche Forschungsgemeinschaft and the "Zentrum für Umweltforschung der Johannes Gutenberg-Universität Mainz" is gratefully acknowledged. Part of the measurements reported in this work were performed at Pacific Northwest National Laboratory with support from the U.S. Department of Energy, Office of Science under Contract DE-AC06-76RLO 1830.

References

1. C.E. Rolfs, W.S. Rodney, *Cauldrons in the Cosmos* (Chicago Press, Chicago and London, 1988), Chap. 9.
2. F. Käppeler, H. Beer, K. Wisshak, Rep. Prog. Phys. **52**, 945 (1989).
3. K. Wisshak, F. Voss, F. Käppeler, K. Guber, L. Kazakov, N. Kornilov, M. Uhl, G. Reffo, Phys. Rev. C **52**, 2762 (1995).
4. F. Käppeler, R. Gallino, M. Busso, G. Picchio, C.M. Raiteri, Astrophys. J. **354**, 630 (1990).
5. *NUDAT database: National Nuclear Data Center* (Brookhaven National Laboratory, USA, 1997).
6. O. Eugster, F. Tera, D.S. Burnett, G.J. Wasserburg, J. Geophys. Res. **75**, 2753 (1970).
7. H. Hidaka, M. Ebihara, M. Shima, Anal. Chem. **67**, 1437 (1995).
8. G. Strich, P.L. Hagan, K.H. Gerber, R.A. Slutsky, Radiology **154**, 723 (1985).
9. R. Mathur-De Vré, M. Lemort, Brit. J. Radiology **68**, 225 (1995).
10. M.I.K. Santala, H.M. Lauranto, T.T. Kajava, R.R.E. Salomaa, in *Proceedings of the Seventh International Symposium on RIS*, Bernkastel-Kues, 1994, edited by H.-J. Kluge *et al.* (AIP Conf. Ser. RIS-94, 1995), Vol. 329, p. 237.
11. M.I.K. Santala, A.S. Daavittila, H.M. Lauranto, R.R.E. Salomaa, Appl. Phys. B **64**, 339 (1997).
12. B.A. Bushaw, F. Juston, W. Nörtershäuser, N. Trautmann, P. Voss-de Haan, K. Wendt, in *Proceedings of the Eighth International Symposium on RIS*, State College, 1996, edited by N. Winograd *et al.* (AIP Conf. Ser. RIS-96, 1997), Vol. 388, p. 115.
13. K. Wendt, K. Blaum, B.A. Bushaw, F. Juston, W. Nörtershäuser, N. Trautmann, B. Wiche, J. Fresenius, Anal. Chem. **359**, 361 (1997).
14. A. Hemmerich, D.H. McIntyre, C. Zimmermann, T.W. Hänsch, Opt. Lett. **15**, 372 (1990).
15. S. Nakamura, W. Kaenders, Laser Focus World 4/99.
16. W.G. Jin, H. Sakata, M. Wakasugi, T. Horiguchi, Y. Yoshizawa, Phys. Rev. A **42**, 1416 (1990).
17. W.J. Childs, Phys. Rev. A **39**, 4956 (1989).
18. M. Wakasugi, T. Horiguchi, W.G. Jin, H. Sakata, Y. Yoshizawa, J. Phys. Soc. Jpn **59**, 2700 (1990).
19. G. Fricke, C. Bernhardt, K. Heilig, L.A. Schaller, L. Schellenberg, E.B. Shera, C.W. De Jager, At. Data Nucl. Data Tables **60**, 117 (1995).
20. W. Nörtershäuser, K. Blaum, K. Icker, P. Müller, A. Schmitt, K. Wendt, B. Wiche, Eur. Phys. J. D **2**, 33 (1998).
21. G. Klemz, Ph.D. thesis, D 83, Technische Universität Berlin, 1995.
22. B.A. Bushaw, G.K. Gerke, in *Proceedings of the Fourth International Symposium on RIS*, Gaithersburg, 1988, edited by T.B. Lucatorto *et al.* (Inst. Phys. Conf. Ser. RIS-88, 1988), Vol. 94 , p. 277.
23. K. Blaum, Ch. Geppert, P. Müller, W. Nörtershäuser, E.W. Otten, A. Schmitt, N. Trautmann, K. Wendt, B.A. Bushaw, Int. J. Mass Spectrom. Ion Processes **181**, 67 (1998).
24. B.A. Bushaw, B.D. Cannon, G.K. Gerke, T.J. Whitaker, Opt. Lett. **11**, 422 (1986).
25. W.Z. Zhao, J.E. Simsarian, L.A. Orozco, G.D. Sprouse, Rev. Sci. Instrum. **69**, 3737 (1998).
26. P. De Bièvre, P.D.P. Taylor, Int. J. Mass Spectrom. Ion Processes **123**, 149 (1993).
27. W. Nörtershäuser, N. Trautmann, K. Wendt, B.A. Bushaw, Spectrochim. Acta B **53**, 709 (1998).
28. P. Brix, H. Kopfermann, Z. Phys. **126**, 344 (1949).
29. H. Kopfermann, *Nuclear moments* (Academic Press, New York, 1958).
30. MINUIT – Function Minimization and Error Analysis Version 92.1, CERN Program Library Entry D506, CERN Geneva, Switzerland (1992).
31. I.I. Sobel'man, *Atomic spectra and radiative transitions* (Springer Verlag, Berlin, 1991).
32. P. Aufmuth, K. Heilig, A. Steudel, At. Data Nucl. Data Tables **37**, 455 (1987).
33. W.H. King, *Isotope Shifts in Atomic Spectra* (Plenum Press, New York/London, 1984).
34. K. Heilig, A. Steudel, At. Data Nucl. Data Tables **14**, 613 (1974).
35. W.C. Martin, R. Zalubas, L. Hagan, *Atomic Energy Levels – The Rare-Earth Elements* (NSRDS-NBS 60, U.S. Department of Commerce, National Bureau of Standards, Washington, 1978).
36. G. Fricke, private communication.
37. S.B. Dutta, A.G. Martin, W.F. Rogers, D.L. Clark, Phys. Rev. C **42**, 1911 (1990).